CMS Physics Analysis Summary

Contact: cms-pag-conveners-heavyions@cern.ch 2020/05/23

Studies of parton-medium interactions using Z-tagged charged particles in PbPb collisions at $\sqrt{s_{\mathrm{NN}}} = 5.02$ TeV

The CMS Collaboration

Abstract

The first measurements of Z boson-tagged charged hadron spectra are reported in PbPb collisions at $\sqrt{s_{\mathrm{NN}}} = 5$ TeV, using the PbPb collision data recorded by the CMS experiment at the LHC in 2018, corresponding to an integrated luminosity of 1.7 nb^{-1}. Hadronic collision data with at least one Z boson with transverse momentum $p_{\mathrm{T}} > 30$ GeV/c are analyzed. The azimuthal angle distributions with respect to the Z bosons, which are sensitive to medium recoils and modification of in-medium parton shower, are measured in PbPb collisions. The results indicate a modification of the angular correlation functions with respect to the reference measured in pp interactions at the same collision energy. The first measurements of Z-tagged fragmentation functions and charged particle p_{T} spectra are also reported. These measurements are sensitive to the modification of the longitudinal structure of the parton shower inside the medium. Significant modifications of the fragmentation functions and charged particle p_{T} spectra are observed.

1 Introduction

Quantum chromodynamics predicts that in relativistic heavy ion collisions a state of deconfined quarks and gluons known as quark-gluon plasma (QGP) can be formed [1, 2]. Parton scatterings with large momentum transfer, which occur very early in the collision compared to the timescale of QGP formation, provide tomographic probes of the plasma [3]. The outgoing partons interact strongly with the QGP and lose energy [4, 5]. This phenomenon, known as "jet quenching", has been observed through measurements of hadrons with high transverse momentum (p_{T}) [6–10] and of jets [11–14], both created by the fragmentation of the high-momentum partons. In contrast, measurements of jets produced in the same hard scattering in conjunction with an electroweak boson (e.g., a photon, Z, or W), which does not interact strongly with the QGP [15–18], have an advantage [19, 20] in that the electroweak boson transverse momentum (p_{T}) reflects, on average, the initial energy of the associated parton that fragments into the jet, before any medium-induced energy loss has occurred [21].

In this note, we report the first measurement of Z-tagged hadron spectra in PbPb and pp collisions. The PbPb and pp collisions at a nucleon-nucleon center-of-mass energy $\sqrt{s_{\mathrm{NN}}} = 5.02\,\mathrm{TeV}$ correspond to integrated luminosities of about $1.7\,\mathrm{nb}^{-1}$ and $304\,\mathrm{pb}^{-1}$, respectively. The goal of the proposed measurement is the following: (1) to study the medium modification of the hadron momentum spectra coming from hard scattered partons tagged by Z bosons; (2) to reveal possible angular decorrelations between the unmodified Z boson and the charged hadrons due to the in-medium transverse momentum broadening; (3) to study the possible effects of medium recoil in the Z-hadron angular correlation functions. This analysis correlates Z bosons (reconstructed in the dilepton decay channel) and charged particle tracks in relative azimuthal angle. The number of tracks per Z boson is studied as a function of the azimuthal angle difference between the Z boson and all other tracks reconstructed in the same event, $\Delta\phi_{\mathrm{trk,Z}} = |\phi^{\mathrm{trk}} - \phi^{\mathrm{Z}}|$. The note also presents the Z-tagged jet fragmentation function, defined as $\xi_{\mathrm{T}}^{\mathrm{Z,trk}} = \ln\left[-|\vec{p}_{\mathrm{T}}^{\,\mathrm{Z}}|^2/(\vec{p}_{\mathrm{T}}^{\,\mathrm{trk}} \cdot \vec{p}_{\mathrm{T}}^{\,\mathrm{Z}})\right]$, where $\vec{p}_{\mathrm{T}}^{\,\mathrm{Z}}$ and $\vec{p}_{\mathrm{T}}^{\,\mathrm{trk}}$ are the p_{T} with respect to the beam direction of the Z boson and track, respectively. For the fragmentation function results only, in order to increase the fraction of the tracks from the recoil of the Z boson used for tagging, tracks are required to be at $\Delta\phi_{\mathrm{trk,Z}} > 7\pi/8$ away from the Z candidate.

2 The CMS detector and event selection

The central feature of the CMS detector is a superconducting solenoid of 6 m internal diameter, providing a magnetic field of 3.8 T. Within the solenoid volume are a silicon pixel and strip tracker, a lead tungstate crystal electromagnetic calorimeter (ECAL), and a brass and scintillator hadron calorimeter (HCAL), each composed of a barrel and two endcap sections. Hadron forward (HF) calorimeters extend the pseudorapidity coverage up to $|\eta| = 5.2$ and are used for event selection. In addition, in the case of PbPb events, the HF signals are used to determine the degree of overlap ("centrality") of the two colliding Pb nuclei [22]. Muons are measured in gas-ionization detectors located outside the solenoid. A more detailed description of the CMS detector can be found in Ref. [23].

The event samples are selected online with dedicated lepton triggers, and cleaned offline to remove noncollision events, such as beam-gas interactions or cosmic-ray muons [10]. The $\mathrm{Z} \to \mathrm{e}^+\mathrm{e}^-$ events are triggered if one ECAL cluster [24] has transverse energy greater than 20 GeV and $|\eta| < 2.1$, while the $\mathrm{Z} \to \mu^+\mu^-$ triggers require one muon of $p_{\mathrm{T}} > 12\,\mathrm{GeV}/c$ and $|\eta| < 2.4$. In addition, events are required to have at least one reconstructed primary interaction vertex, and at least two towers with total energy greater than 4 GeV each on each side of the

HFs. The average pileup (the mean of the number of collisions within the same crossing) is 2 in pp, and negligible in PbPb collisions. For PbPb collisions, the results are presented in four centrality intervals, 0–30, 30–50, 50–90, and 70–90%. Centrality is determined by the total energy deposited in the HFs, starting at 0% for the most central collisions, and is evaluated as percentiles of the distribution of the energy deposited in the HF calorimeters [22].

3 Simulation and physics object reconstruction

The PYTHIA 8.212 [25] Monte Carlo (MC) event generator, with tune CP5 [26], and MADGRAPH5_aMC@NLO 8.212 [27] next-to-leading order (NLO) generators are used to simulate Z+jet signal events. In the PbPb case, "embedded" samples are created by embedding PYTHIA and MADGRAPH5_aMC@NLO signal events in heavy ion events generated with the HYDJET 1.9 MC event generator [28]. The generated events are propagated through the CMS apparatus using the GEANT 4 package [29].

Electrons are identified as ECAL superclusters [30] matched in position and energy to tracks reconstructed in the tracker. They must have $p_{\mathrm{T}} > 20\,\mathrm{GeV}/c$ and each supercluster must be within the acceptance of the trigger, $|\eta| < 2.1$. Electron candidates in the transition region between the barrel and endcap subdetectors ($1.44 < |\eta| < 1.57$) are excluded from both pp and PbPb samples. For PbPb data, an additional region ($\eta < -1.39$ and $-1.6 < \phi < -0.9$) is excluded because of corresponding calorimeter modules being inactive. A narrow transverse shape of showers in the ECAL and a low HCAL over ECAL energy ratio are required to reject misidentified electrons. Additional tracking information is used to distinguish electrons from charged hadrons [30].

Muons are selected by requiring segments in at least two muon detector planes and a good-quality fit when connecting them to tracker segments. A minimum number of hits in the pixel and strip layers is required, and the reconstructed muon tracks must point to the primary vertex in the transverse and longitudinal directions [31]. This suppresses hadronic punch-through and muons from in-flight decays of hadrons. The same selections are applied for both pp and PbPb data. In order to suppress the background continuum under the Z peak, mostly originating from uncorrelated simultaneous decays of heavy flavour mesons, the muons are required to have $p_{\mathrm{T}} > 20\,\mathrm{GeV}/c$. In addition, the muon tracks must fall within the acceptance of the muon detectors, $|\eta^{\mu}| < 2.4$.

The track reconstruction used in pp and PbPb collisions is described in Ref. [32]. Corrections for tracking efficiency, detector acceptance, and misreconstruction rate are obtained following the procedure in Ref. [10]. Additional corrections are applied for the residual tracking efficiency difference seen between HYDJET and embedded MADGRAPH5_aMC@NLO samples. The selection criteria are the same as in Ref. [10] for both pp and PbPb data.

The Z candidates are defined as electron or muon pairs, with a reconstructed invariant mass ($M^{\ell\ell}$) in the interval $60\text{–}120\,\mathrm{GeV}/c^2$ and $p_{\mathrm{T}}^{\mathrm{Z}} > 30\,\mathrm{GeV}/c$. Electron and muon pairs are combined after being corrected for acceptance and reconstruction, identification, and trigger efficiencies. The wider muon rapidity acceptance makes the relative contribution from muon pairs slightly higher. Each Z candidate is paired with all tracks in the same event that pass the $p_{\mathrm{T}}^{\mathrm{trk}} > 1\,\mathrm{GeV}/c$ and $|\eta^{\mathrm{trk}}| < 2.4$ selection. To eliminate the contamination of leptons from Z decays, the radial distance between a track and a lepton from the Z decay is required to be greater than 0.02. Results are obtained separately for Z candidates from oppositely-charged electron or muon pairs, corrected for the individual lepton efficiency, and subtracted for the relative contribution from same charge pairs in order to minimize the residual contribution from physics processes

W+jet, $\mathrm{t\bar{t}}$, QCD jet, and $\mathrm{Z} \to \tau\tau$ events. After this, the two channels are combined and treated as one.

4 Data analysis

Combinatorial background originating from tracks from the underlying event (UE) in PbPb collisions is subtracted to obtain the correlation between the Z boson candidate and tracks that are produced in the same hard scattering. The background is estimated from data with an event mixing procedure, similar to those in Refs. [33, 34], where the Z boson is paired with tracks found in events chosen randomly from a minimum-bias (MB) PbPb dataset with similar event characteristics (energy deposited in the HF after accounting for the UE, and interaction vertex position). Events are split into bins of total HF energy, E^{HF}, where the bin width is 150 GeV. To ensure that the Z events and MB events have the same level of the UE, a Z event with total HF energy $E^{\mathrm{HF,\,Z}}$ is paired with MB events which are in the same E^{HF} interval as events with $E^{\mathrm{HF}} = E^{\mathrm{HF,\,Z}} - \langle E^{\mathrm{HF,\,Z,\,pp}} \rangle$. The $\langle E^{\mathrm{HF,\,Z,\,pp}} \rangle$ is the average of E^{HF} over events in pp data where a Z boson is produced and there is no additional pp interaction. The normalization of the combinatorial background is given by the number of MB events used. The event-by-event deviation of the number of UE tracks before subtraction can be much larger than the number of tracks after subtraction. In order to reflect this statistical effect of the UE, the statistical uncertainties of the PbPb distributions are calculated using the bootstrap method [35], where events are resampled 400 times.

5 Systematic uncertainties

Several systematic uncertainties are considered, to account for uncertainties related to the tracking efficiency and corrections, pileup, background subtraction, lepton efficiency and energy scale, and disagreements seen between reconstructed and generated particles. No significant differences are seen between results from electron and muon pairs. Systematic uncertainties, except for lepton efficiency and energy scale, are not significantly different between electron and muon pairs.

The uncertainty related to the tracking efficiency is estimated as the difference in the track reconstruction efficiency between data and simulation [10]. It is 5 (2.4)% for PbPb (pp) data, for all of $\Delta\phi_{\mathrm{trk,Z}}$, $\xi_{\mathrm{T}}^{\mathrm{Z,trk}}$, and $p_{\mathrm{T}}^{\mathrm{trk}}$. The uncertainty related to the additional corrections is obtained by comparing corrections obtained from embedded samples. On average, it is 2.7%, 2.7%, 2.5%, for $\Delta\phi_{\mathrm{trk,Z}}$, $\xi_{\mathrm{T}}^{\mathrm{Z,trk}}$, and $p_{\mathrm{T}}^{\mathrm{trk}}$ in 0–30% centrality PbPb collisions. Systematic uncertainties are quoted for the disagreements seen in the comparison of observables constructed using corrected tracks and generated charged particles. The amount of disagreement is quoted as a systematic uncertainty, being on average 8.1 (0.7)%, 5 (2.3)%, and 3.8 (1.7)% for $\Delta\phi_{\mathrm{trk,Z}}$, $\xi_{\mathrm{T}}^{\mathrm{Z,trk}}$, and $p_{\mathrm{T}}^{\mathrm{trk}}$ in 0–30% centrality PbPb (pp) collisions, respectively.

No corrections were applied to remove the residual pileup effects in pp data. Nominal distributions (no requirement on pileup) are compared to those from events without pileup; differences are on average 1.3%, 1.9%, and 2.0% for $\Delta\phi_{\mathrm{trk,Z}}$, $\xi_{\mathrm{T}}^{\mathrm{Z,trk}}$, and $p_{\mathrm{T}}^{\mathrm{trk}}$, respectively, and quoted as a systematic uncertainty. The event mixing procedure was repeated by shifting the $\langle E^{\mathrm{HF,\,Z,\,pp}} \rangle$ by 5%, the maximum difference in the HF response between pp and PbPb data taking periods. Differences from the nominal procedure for $\Delta\phi_{\mathrm{trk,Z}}$, $\xi_{\mathrm{T}}^{\mathrm{Z,trk}}$, and $p_{\mathrm{T}}^{\mathrm{trk}}$ in 0–30% centrality PbPb are on average 3.0%, 1.8%, and 0.8%, respectively.

Lepton efficiencies are varied by the uncertainty in their data-to-MC differences and the dif-

ferences from nominal distributions are quoted as systematic uncertainty. These uncertainties are 0.7 (0.4)% for 0–30% centrality PbPb (pp). The p_{T} of leptons is shifted by their energy correction uncertainties; the resulting uncertainties are 1.7 (0.1)%, 2.6 (0.4)%, and 1.7 (0.2)% for $\Delta\phi_{\mathrm{trk,Z}}$, $\xi_{\mathrm{T}}^{\mathrm{Z,trk}}$, and $p_{\mathrm{T}}^{\mathrm{trk}}$ in 0–30% centrality PbPb (pp), respectively.

6 Results

The distributions of the azimuthal angle difference between charged particles and Z bosons, normalized by the number of Z bosons in each dataset (and for the PbPb case, in each centrality interval), are shown in Fig. 1. This type of angular correlation function could reveal medium modification of the away-side ($\Delta\phi_{\mathrm{trk,Z}} \sim \pi$) jet constituents, and, on the same-side ($\Delta\phi_{\mathrm{trk,Z}} < \pi/2$), effects of medium recoil and medium response predicted by some theoretical calculations [36].

The distribution in pp collisions is peaked at $\Delta\phi_{\mathrm{trk,Z}} \sim \pi$, the signature of an away-side jet recoiling off the Z boson. The PbPb data, after background subtraction, shows an excess in the number of associated particles with respect to the pp reference. To quantify the size of the excess, the difference between the PbPb and pp results is calculated and shown in Fig. 1. An enhancement of particle production is observed in 0–30%, 30–50%, and 50–70% PbPb collisions with respect to the pp reference. This could be caused by medium response, or by the quenching of associated jets in Z+multi-jet events [37]. Finally, the enhanced production of associated particles disappears when looking in the peripheral (i.e., the most pp-like) 70–90% centrality interval.

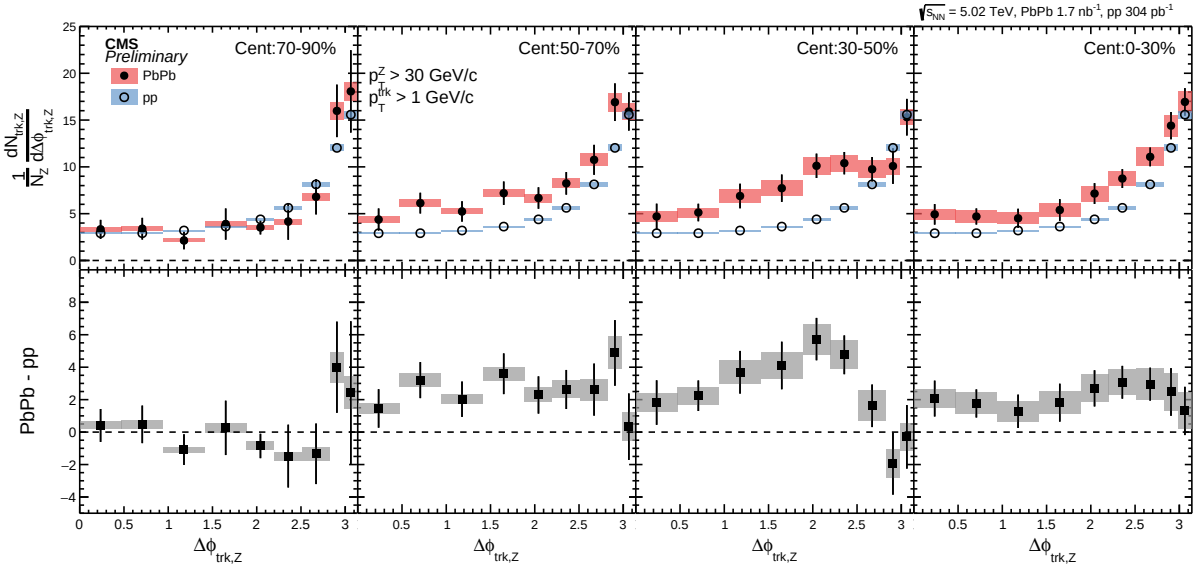

Figure 1: Top : Distributions of $\Delta\phi_{\mathrm{trk,Z}}$ in pp collisions compared to PbPb collisions in 70–90% (left) 50–70%, 30–50%, and 0–30% (right) centrality intervals. Bottom : Difference between the PbPb and pp distributions. The vertical bars through the points represent statistical uncertainties, while the shaded boxes indicate systematic uncertainties.

To study the fragmentation function of the parton recoiling the Z boson, the $\xi_{\mathrm{T}}^{\mathrm{Z,trk}}$ distributions are measured in PbPb and, for reference, also in pp data. For these results, shown in Figs. 2 and 3, tracks are required to satisfy $\Delta\phi_{\mathrm{trk,Z}} > 7\pi/8$. All distributions are normalized by the number of Z bosons measured in each dataset. In Fig. 2, the low and high $\xi_{\mathrm{T}}^{\mathrm{Z,trk}}$ regions correspond to high- and low-p_{T} particles, respectively. No significant modification is observed in the 70–90% centrality PbPb collisions. In more central collisions, charged particles in the $\xi_{\mathrm{T}}^{\mathrm{Z,trk}} < 3$ interval are suppressed, whereas an enhancement is observed for $\xi_{\mathrm{T}}^{\mathrm{Z,trk}} > 3$, a similar finding as observed with a photon-tagged jet substructure measurement [33].

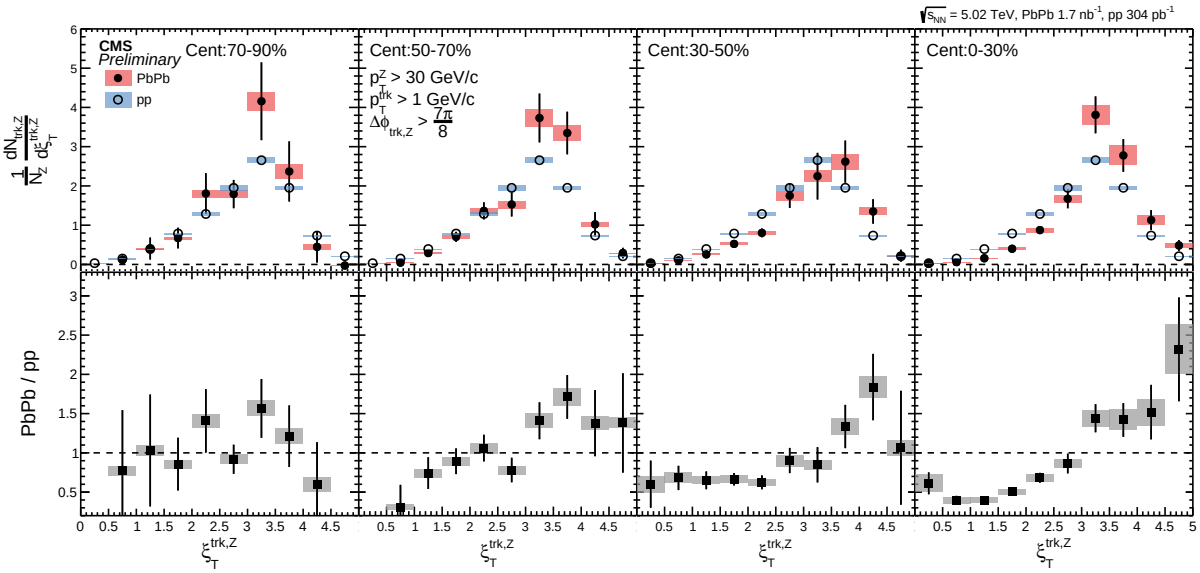

Figure 2: Top : Distributions of $\xi_{\mathrm{T}}^{\mathrm{Z,trk}}$ in pp collisions compared to PbPb collisions in 70–90% (left), 50–70% , 30–50%, and 0–30% (right) centrality intervals. Bottom : ratio of the PbPb and pp distributions. The vertical bars through the points represent statistical uncertainties, while the shaded boxes indicate systematic uncertainties.

Similar to the nuclear modification factor measurements, one can extract the modification of the charged particle p_{T} spectra by comparing the per-Z boson associated yields in pp and PbPb collisions. Figure 3 shows these distributions as a function of $p_{\mathrm{T}}^{\mathrm{trk}}$ in pp and PbPb data, together with their ratio. In the most peripheral event class, there is no significant modification of the charged particle p_{T} spectrum in PbPb collisions. In more central events, at high p_{T}, the particle production is suppressed in PbPb compared to the pp reference data. In the same time, at low p_{T} ($1 < p_{\mathrm{T}}^{\mathrm{trk}} < 2\,\mathrm{GeV}/c$), an enhancement is observed consistent with the one seen in $\Delta\phi_{\mathrm{trk,Z}}$ results. Modifications of the $\xi_{\mathrm{T}}^{\mathrm{Z,trk}}$ and $p_{\mathrm{T}}^{\mathrm{trk}}$ distributions are largest in the 0–30% centrality interval indicating the strongest medium effects.

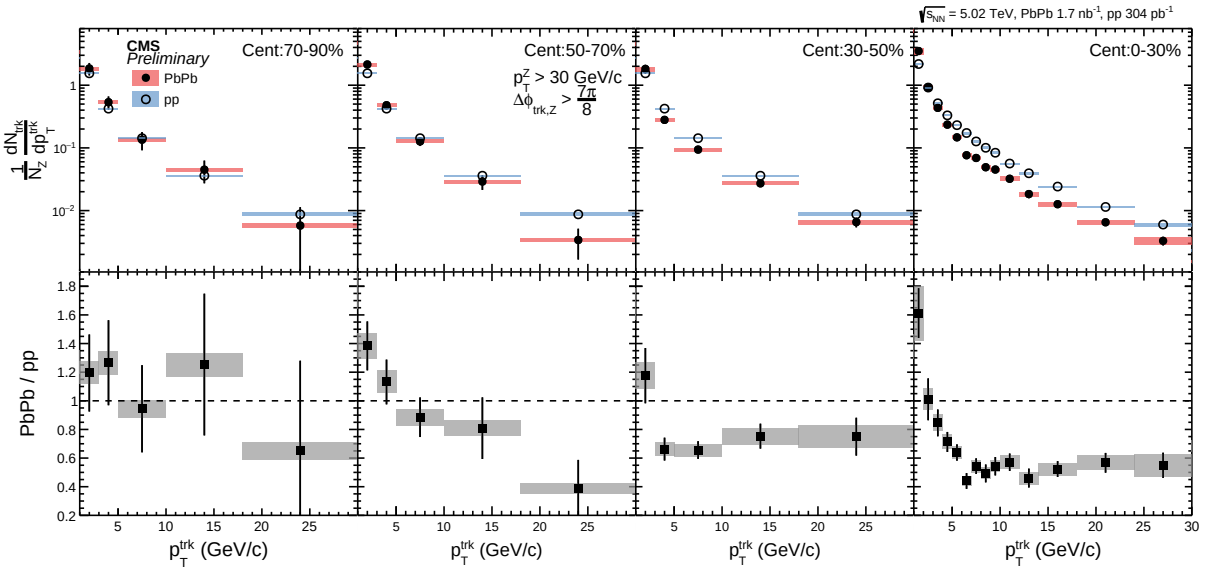

Figure 3: Top : Distributions of $p_{\mathrm{T}}^{\mathrm{trk}}$ in pp collisions compared to PbPb collisions in 70–90% (left) 50–70%, 30–50%, and 0–30% (right) centrality intervals. Bottom : ratio of the PbPb and pp distributions. The vertical bars through the points represent statistical uncertainties, while the shaded boxes indicate systematic uncertainties.

7 Summary

In summary, the first measurements of Z-tagged charged hadron spectra are reported in PbPb collisions at $\sqrt{s_{\mathrm{NN}}} = 5.02$ TeV, using the data collected in 2018. The corresponding integrated luminosity of the PbPb data is 1.7 nb^{-1}, which made the analysis possible for the first time. Collision data with at least one Z boson with $p_{\mathrm{T}}^{\mathrm{Z}} > 30$ GeV/c are analyzed. The azimuthal angle distributions with respect to the Z bosons, which are sensitive to the modification of in-medium parton shower and medium recoils, are measured in PbPb collisions. Comparison of the PbPb results to the reference pp results indicates a modification of the angular correlation functions. This modification extends to azimuthal angles close to the Z boson in most central PbPb events. The first measurement of Z-tagged fragmentation functions and $p_{\mathrm{T}}^{\mathrm{trk}}$ spectra, which are sensitive to the modification of the longitudinal structure of the parton shower inside the medium, are also reported. Significant modifications of the fragmentation functions and $p_{\mathrm{T}}^{\mathrm{trk}}$ spectra coming from the recoiled partons are observed. These results are complementary to the measurements using inclusive jets, dijet and photon-tagged jet events.

References

[1] J. C. Collins and M. J. Perry, "Superdense matter: Neutrons or asymptotically free quarks?", *Phys. Rev. Lett.* **34** (1975) 1353, doi:10.1103/PhysRevLett.34.1353.

[2] F. Karsch, "The phase transition to the quark gluon plasma: recent results from lattice calculations", *Nucl. Phys. A* **590** (1995) 367, doi:10.1016/0375-9474(95)00248-Y, arXiv:hep-lat/9503010.

[3] D. A. Appel, "Jets as a probe of quark-gluon plasmas", *Phys. Rev. D* **33** (1986) 717, doi:10.1103/PhysRevD.33.717.

[4] J. P. Blaizot and L. D. McLerran, "Jets in expanding quark-gluon plasmas", *Phys. Rev. D* **34** (1986) 2739, doi:10.1103/PhysRevD.34.2739.

[5] M. Gyulassy and M. Plümer, "Jet quenching in dense matter", *Phys. Lett. B* **243** (1990) 432, doi:10.1016/0370-2693(90)91409-5.

[6] STAR Collaboration, "Transverse-momentum and collision-energy dependence of high-p_{t} hadron suppression in Au+Au collisions at ultrarelativistic energies", *Phys. Rev. Lett.* **91** (2003) 172302, doi:10.1103/PhysRevLett.91.172302, arXiv:nucl-ex/0305015.

[7] PHENIX Collaboration, "Suppression pattern of neutral pions at high transverse momentum in Au+Au collisions at $\sqrt{s_{\mathrm{NN}}} = 200$ GeV and constraints on medium transport coefficients", *Phys. Rev. Lett.* **101** (2008) 232301, doi:10.1103/PhysRevLett.101.232301, arXiv:0801.4020.

[8] ALICE Collaboration, "Centrality dependence of charged particle production at large transverse momentum in Pb–Pb collisions at $\sqrt{s_{\mathrm{NN}}} = 2.76$ TeV", *Phys. Lett. B* **720** (2013) 52, doi:10.1016/j.physletb.2013.01.051, arXiv:1208.2711.

[9] ATLAS Collaboration, "Measurement of charged-particle spectra in Pb+Pb collisions at $\sqrt{s_{\mathrm{NN}}} = 2.76$ TeV with the ATLAS detector at the LHC", *JHEP* **09** (2015) 050, doi:10.1007/JHEP09(2015)050, arXiv:1504.04337.

[10] CMS Collaboration, "Charged-particle nuclear modification factors in PbPb and pPb collisions at $\sqrt{s_{\mathrm{NN}}} = 5.02$ TeV", *JHEP* **04** (2017) 039, doi:10.1007/JHEP04(2017)039, arXiv:1611.01664.

[11] CMS Collaboration, "Measurement of inclusive jet cross sections in pp and PbPb collisions at $\sqrt{s_{\mathrm{NN}}} = 2.76$ TeV", *Phys. Rev. C* **96** (2017) 015202, doi:10.1103/PhysRevC.96.015202, arXiv:1609.05383.

[12] ATLAS Collaboration, "Centrality and rapidity dependence of inclusive jet production in $\sqrt{s_{\mathrm{NN}}} = 5.02$ TeV proton–lead collisions with the ATLAS detector", *Phys. Lett. B* **748** (2015) 392, doi:10.1016/j.physletb.2015.07.023, arXiv:1412.4092.

[13] ALICE Collaboration, "Measurement of jet quenching with semi-inclusive hadron-jet distributions in central Pb-Pb collisions at $\sqrt{s_{\mathrm{NN}}} = 2.76$ TeV", *JHEP* **09** (2015) 170, doi:10.1007/JHEP09(2015)170, arXiv:1506.03984.

[14] STAR Collaboration, "Dijet imbalance measurements in Au+Au and pp collisions at $\sqrt{s_{\mathrm{NN}}} = 200$ GeV at STAR", *Phys. Rev. Lett.* **119** (2017) 062301, doi:10.1103/PhysRevLett.119.062301, arXiv:1609.03878.

[15] ATLAS Collaboration, "Centrality, rapidity and transverse momentum dependence of isolated prompt photon production in lead-lead collisions at $\sqrt{s_{\mathrm{NN}}} = 2.76$ TeV measured with the ATLAS detector", *Phys. Rev. C* **93** (2016) 034914, doi:10.1103/PhysRevC.93.034914, arXiv:1506.08552.

[16] CMS Collaboration, "Measurement of isolated photon production in pp and PbPb collisions at $\sqrt{s_{\mathrm{NN}}} = 2.76$ TeV", *Phys. Lett. B* **710** (2012) 256, doi:10.1016/j.physletb.2012.02.077, arXiv:1201.3093.

[17] CMS Collaboration, "Study of W boson production in PbPb and pp collisions at $\sqrt{s_{\mathrm{NN}}} = 2.76$ TeV", *Phys. Lett. B* **715** (2012) 66, doi:10.1016/j.physletb.2012.07.025, arXiv:1205.6334.

[18] CMS Collaboration, "Study of Z production in PbPb and pp collisions at $\sqrt{s_{\mathrm{NN}}} = 2.76$ TeV in the dimuon and dielectron decay channels", *JHEP* **03** (2015) 022, doi:10.1007/JHEP03(2015)022, arXiv:1410.4825.

[19] V. Kartvelishvili, R. Kvatadze, and R. Shanidze, "On Z and Z+jet production in heavy ion collisions", *Phys. Lett. B* **356** (1995) 589, doi:10.1016/0370-2693(95)00865-I, arXiv:hep-ph/9505418.

[20] X.-N. Wang, Z. Huang, and I. Sarcevic, "Jet quenching in the opposite direction of a tagged photon in high-energy heavy ion collisions", *Phys. Rev. Lett.* **77** (1996) 231, doi:10.1103/PhysRevLett.77.231, arXiv:hep-ph/9605213.

[21] Z.-B. Kang, I. Vitev, and H. Xing, "Vector-boson-tagged jet production in heavy ion collisions at energies available at the CERN large hadron collider", *Phys. Rev. C* **96** (2017) 014912, doi:10.1103/PhysRevC.96.014912, arXiv:1702.07276.

[22] CMS Collaboration, "Observation and studies of jet quenching in PbPb collisions at $\sqrt{s_{\mathrm{NN}}} = 2.76$ TeV", *Phys. Rev. C* **84** (2011) 024906, doi:10.1103/PhysRevC.84.024906, arXiv:1102.1957.

[23] CMS Collaboration, "The CMS experiment at the CERN LHC", *JINST* **3** (2008) S08004, doi:10.1088/1748-0221/3/08/S08004.

[24] CMS Collaboration, "The CMS trigger system", *JINST* **12** (2017) P01020, doi:10.1088/1748-0221/12/01/P01020, arXiv:1609.02366.

[25] T. Sjöstrand, S. Mrenna, and P. Z. Skands, "A brief introduction to PYTHIA 8.1", *Comput. Phys. Commun.* **178** (2008) 852, doi:10.1016/j.cpc.2008.01.036, arXiv:0710.3820.

[26] CMS Collaboration, "Extraction and validation of a new set of CMS PYTHIA8 tunes from underlying-event measurements", *Eur. Phys. J. C* **80** (2020) doi:10.1140/epjc/s10052-019-7499-4, arXiv:1903.12179.

[27] J. Alwall et al., "The automated computation of tree-level and next-to-leading order differential cross sections, and their matching to parton shower simulations", *JHEP* **07** (2014) 079, doi:10.1007/JHEP07(2014)079, arXiv:1405.0301.

[28] I. P. Lokhtin and A. M. Snigirev, "A model of jet quenching in ultrarelativistic heavy ion collisions and high-p_{T} hadron spectra at RHIC", *Eur. Phys. J. C* **45** (2006) 211, doi:10.1140/epjc/s2005-02426-3, arXiv:hep-ph/0506189.

[29] GEANT4 Collaboration, "GEANT4—a simulation toolkit", *Nucl. Instrum. Meth. A* **506** (2003) 250, doi:10.1016/S0168-9002(03)01368-8.

[30] CMS Collaboration, "Performance of Electron Reconstruction and Selection with the CMS Detector in Proton-Proton Collisions at $\sqrt{s} = 8$ TeV", *JINST* **10** (2015), no. 06, P06005, doi:10.1088/1748-0221/10/06/P06005, arXiv:1502.02701.

[31] CMS Collaboration, "Performance of CMS Muon Reconstruction in pp Collision Events at $\sqrt{s} = 7$ TeV", *JINST* **7** (2012) P10002, doi:10.1088/1748-0221/7/10/P10002, arXiv:1206.4071.

[32] CMS Collaboration, "Description and performance of track and primary-vertex reconstruction with the CMS tracker", *JINST* **9** (2014) P10009, doi:10.1088/1748-0221/9/10/P10009, arXiv:1405.6569.

[33] CMS Collaboration, "Observation of Medium-Induced Modifications of Jet Fragmentation in Pb-Pb Collisions at $\sqrt{s_{\mathrm{NN}}} = 5.02$ TeV Using Isolated Photon-Tagged Jets", *Phys. Rev. Lett.* **121** (2018), no. 24, 242301, doi:10.1103/PhysRevLett.121.242301, arXiv:1801.04895.

[34] CMS Collaboration, "Jet Shapes of Isolated Photon-Tagged Jets in Pb-Pb and pp Collisions at $\sqrt{s_{\mathrm{NN}}} = 5.02$ TeV", *Phys. Rev. Lett.* **122** (2019), no. 15, 152001, doi:10.1103/PhysRevLett.122.152001, arXiv:1809.08602.

[35] B. Efron, "Bootstrap methods: Another look at the jackknife", *Ann. Statist.* **7** (1979), no. 1, doi:10.1214/aos/1176344552.

[36] W. Chen et al., "Effects of jet-induced medium excitation in γ-hadron correlation in A+A collisions", *Phys. Lett. B* **777** (2018) 86, doi:10.1016/j.physletb.2017.12.015, arXiv:1704.03648.

[37] R. Kunnawalkam Elayavalli and K. C. Zapp, "Medium response in JEWEL and its impact on jet shape observables in heavy ion collisions", *JHEP* **07** (2017) 141, doi:10.1007/JHEP07(2017)141, arXiv:1707.01539.